Chinese Journal of Natural Medicines 24 (2026) 987-998

Contents lists available at ScienceDirect

Chinese Journal of Natural Medicines

journal homepage: www.cjnmcpu.com/

Original article

Comorbid depression exacerbates *Gelsemium elegans* toxicity *via* disruption of the *Clostridium*-LCA-PXR-CYP3A11 metabolic axis

Fugui Zhang[a,Δ], Wanyu Hu[a,Δ], Xiaojie Zhao[a], Bingxuan Fu[a], Yating Lin[a], Cong Xie[b], Ruopeng Yang[a], Yufang Fu[a], Weiling Tan[a], Ling Ye[a,*]

[a] *NMPA Key Laboratory for Research and Evaluation of Drug Metabolism & Guangdong Provincial Key Laboratory of New Drug Screening, School of Pharmaceutical Sciences, Southern Medical University, Guangzhou 510515, China*

[b] *Clinical Pharmacy Center, Nanfang Hospital, Southern Medical University, Guangzhou 510515, China*

ARTICLE INFO

Article history:
Received 17 October 2025
Revised 23 November 2025
Accepted 4 January 2026
Available online 20 August 2026

Keywords:
Gelsemium elegans
Humantenmine
Gut microbiota
Pregnane X receptor
Depression
Neurotoxicity

ABSTRACT

Gelsemium elegans (*G. elegans*) is a toxic medicinal plant traditionally used to treat chronic pain, with its toxicity linked to indole alkaloids such as gelsemine and humantenmine (HMT). Chronic pain often co-occurs with depression, a condition known to disrupt host-microbiota interactions, potentially affecting drug metabolism and toxicity. However, the impact of comorbid depression on the toxicity of *G. elegans* remains unclear. This study investigates how depression exacerbates the neurotoxicity of *G. elegans* and explores the role of the gut microbiota–host metabolic axis in this process. Depression-model mice were treated with *G. elegans* aqueous extract, gelsemine and HMT. Multi-omics approaches, including 16S rRNA sequencing and shotgun metagenomics, were used to analyze microbiota changes under depressive conditions. Functional validation was performed using pseudo-germ-free mice, fecal microbiota transplantation, and supplementation with *Clostridium* species and lithocholic acid (LCA), as well as pregnane X receptor (*Pxr*) knockout models. The results showed that depression significantly heightened the neurotoxicity of *G. elegans*, gelsemine and HMT. Mechanistically, depression reduced *Clostridium* abundance and LCA levels, impairing PXR activation and downregulating hepatic CYP3A11 expression. This disruption of the *Clostridium*-LCA-PXR-CYP3A11 axis hindered the detoxification of indole alkaloids, leading to increased systemic exposure and exacerbated neurotoxicity. Restoration of this pathway through *Clostridium* or LCA supplementation alleviated the toxicity. These findings highlight the role of the *Clostridium*-LCA-PXR-CYP3A11 axis in the altered toxicity of *G. elegans* in a depressive state, and suggest that *Clostridium* species and their metabolites may serve as a potential strategy for mitigating toxicity.

1. Introduction

Gelsemium elegans Benth. (*G. elegans*), a highly toxic medicinal plant native to Southeast Asia, has been traditionally used to treat chronic pain [1-3]. Its pharmacological effects are primarily attributed to its major indole alkaloids, such as gelsemine, humantenmine (HMT) and koumine [4, 5]. These alkaloids exert remarkable analgesic activity by acting on central pathways such as glycine receptors and neurosteroid signaling [6, 7]. Because of their efficacy, these indole alkaloids have been proposed as promising opioid alternatives, with the potential to overcome limitations of current opioid treatments, such as addiction and tolerance [8, 9]. Nevertheless, the clinical use of *G. elegans* is severely constrained by its dose-dependent neurotoxicity, which manifests as symptoms such as dizziness, ataxia, and respiratory suppression [10]. Previous studies have reported that the LD_{50} of *G. elegans* aqueous extract is approximately 15 mg·kg^{-1} [11]. The LD_{50} values of gelsemine and HMT in mice are 56.2 and 0.185 mg·kg^{-1}, respectively [12].

Chronic pain, a major indication for *G. elegans*, frequently coexists with depression, affecting approximately 30%–50% of patients with depression [13, 14]. Disease states can profoundly alter drug efficacy and toxicity. For example, inflammatory diseases downregulate cytochrome P450 enzymes, thereby enhancing the hepatotoxicity of acetaminophen [15], and diabetes increases susceptibility to doxorubicin-induced cardiotoxicity through metabolic remodeling [16]. Previous research has demonstrated that depression can markedly influence the efficacy and safety of traditional herbal medicines. For instance, clinical case reports have documented acute liver failure in depressed patients after consuming *Polygonum multiflorum*, likely due to depression-associated suppression of CYP1A2 activity, which promotes accumulation of hepatotoxic anthraquinones [17]. Similarly, the efficacy of paeoniflorin depends on its gut microbiota-mediated conversion to benzoylpaeoniflorin, a process reduced under depressive conditions owing to altered microbial composition [18]. Furthermore, the metabolism and therapeutic outcomes of antidepressants, such as selective serotonin reuptake inhibitors, are also affected by depression-associated microbial dysbiosis [19].

* Corresponding author.
E-mail address: yeling623@hotmail.com (L. Ye)
Δ These authors contributed equally to this work.

https://doi.org/10.1016/S1875-5364(26)61197-1

Recent studies have highlighted the pivotal role of gut microbiota in modulating drug efficacy and toxicity [20-22]. The gut microbiota can directly modify drug activity through enzymatic reactions or indirectly regulate host drug-metabolizing enzymes *via* microbial metabolites, thereby influencing both drug efficacy and safety [23, 24]. Key microbial metabolites, including secondary bile acids, short-chain fatty acids, and indole derivatives, can activate nuclear receptors such as pregnane X receptor (*Pxr*) and constitutive androstane receptor (*Car*), thereby regulating hepatic CYP450 and phase II enzyme expression [25, 26]. Depression-associated microbial dysbiosis—characterized by reduced *Firmicutes* and increased *Proteobacteria*—may impair these pathways, limit host detoxification capacity, and disrupt drug bioactivation or inactivation, while also altering brain–gut signaling and contributing to behavioral and cognitive dysfunction [27]. Dysbiosis under depressive conditions may further reduce the formation of active or detoxified metabolites, thereby altering the metabolism and efficacy of both conventional drugs and herbal medicines. Together, these observations suggest that depression can significantly modify the metabolism and toxicity of drugs and herbal compounds. However, whether comorbid depressive states exacerbate the neurotoxicity of *G. elegans* remains unknown. Elucidating the underlying microbiota-host metabolic mechanisms may provide critical insights into the safe use of this toxic but pharmacologically valuable medicinal plant.

In this study, we explore how comorbid depression alters the microbiota-host metabolic axis and exacerbates the toxicity of *G. elegans*. We found that depression reduced the abundance of the key bacterium *Clostridium* and its metabolite lithocholic acid (LCA), leading to suppression of the PXR-CYP3A11 pathway. This impairment hindered the metabolism of *G. elegans* alkaloids, resulting in accumulation of the parent compounds and increased neurotoxicity. Supplementation with *Clostridium* or LCA restored PXR-CYP3A11 activity, promoted alkaloid metabolism, and alleviated toxicity. These findings reveal a novel mechanism by which depression modulates drug metabolism and toxicity, providing critical insights for the safety evaluation of traditional medicinal plants.

2. Materials and methods

2.1. Chemicals and reagents

Humantenmine (HMT, JOT-10444, purity > 98%), gelsemine (JOT-10563, purity > 98%), koumine (JOT-10562, purity > 98%) were purchased from Chengdu Pufeide Biotech Co., Ltd. (Chengdu, China). Testosterone (MB1636, purity > 98%) was purchased from MeilunBio Biotech Co., Ltd. (Dalian, China). 6*β*-OH-testosterone (B70332, purity > 98%), ursodeoxycholic acid (UDCA, B21405, purity > 98%), chenodeoxycholic acid (CDCA, B20347, purity > 98%), deoxycholic acid (DCA, B21032, purity > 98%), deoxycholic acid-d_4 (DCA-d_4, S22163, purity > 98%), and lithocholic acid (LCA, B28100, purity > 98%) were purchased from Shanghai Yuanye Biotech Co., Ltd. (Shanghai, China). All remaining reagents were of analytical grade or higher and obtained from commercial suppliers.

2.2. Animals

Male C57BL/6J mice, 6–8 weeks old, were obtained from Sipeifu Biotechnology Co., Ltd. [Beijing, China; License number: SCXK (Jing) 2024-0001]. Male *Pxr* knockout mice, 6–8 weeks old, on a C57BL/6J genetic background were generously provided by West China Hospital, Sichuan University (Chengdu, China) [28]. All experimental animals were housed in a specific pathogen-free (SPF) facility under controlled conditions (24 ± 1 °C, 12 h light/dark cycle). Animal experiments were performed using protocols approved by the Institutional Animal Care and Use Committee of Southern Medical University (Guangzhou, China; Approval No. SMUL202402029).

2.3. Spared nerve injury (SNI)

The SNI procedure was performed as previously described [29]. Mice were briefly anesthetized with isoflurane, and a longitudinal incision was created proximal to the knee with a surgical scalpel to reveal the sciatic nerve. Careful ligation and transection of the common peroneal and tibial nerves were performed distal to the ligation site, followed by excision of a 3 mm segment from the distal stump, whereas the sural nerve was left unaltered. Sham-operated control mice underwent identical surgical procedures without nerve injury. Mice were monitored for 28 days following surgery, and behavioral outcomes of the nerve injury were evaluated using the mechanical withdrawal test (MWT) [30]. In brief, the plantar surface of the mouse hind paw was gently stimulated perpendicularly with a 0.04 g von Frey filament, and withdrawal responses were noted. A paw withdrawal response to the stimulus was considered positive, whereas absence of a response was regarded as negative. Depending on the outcome, von Frey filaments of lower or higher force were subsequently applied.

2.4. Chronic restraint stress

Chronic restraint stress was conducted following our previously described protocols [31]. Specifically, mice were restrained in a plastic holder that restricted their movement without applying pressure for 6 h daily for 28 days. To assess depressive-like behaviors, we recorded immobility time in both the tail suspension test (TST) and the forced swimming test (FST), in which prolonged immobility time reflects a greater severity of depression-like states. In the TST, the tip of each mouse's tail was secured with adhesive tape, and the mouse was suspended approximately 30 cm above the floor. In the FST, each mouse was placed individually in a transparent cylindrical container (10 cm × 10 cm × 25 cm) filled with water maintained at 22–24 °C. Both tests lasted 6 min, and immobility time during the final 4 min was recorded for analysis [32]. All behaviors were video-recorded, and immobility time was manually scored by two experimenters blinded to the groups. Immobility was defined as the absence of active struggling in the TST, with the mouse hanging passively in a vertical, head-down position, and as the cessation of active swimming or climbing in the FST, with the mouse floating and making only minimal movements to keep its head above the water without forward progression.

2.5. SNI combined with chronic restraint stress

Mice underwent SNI surgery, and from postoperative day 4, chronic restraint stress was applied daily for 28 consecutive days to induce a depression model. Behavioral outcomes resulting from nerve injury and stress were evaluated using the MWT, TST, and FST.

2.6. Gut microbiota depletion

A cocktail of antibiotics was administered in the drinking water for two weeks to deplete gut microbiota. The solution contained ampicillin (0.5 g·L^{-1}, MB1378), neomycin (0.5 g·L^{-1}, MB1716), vancomycin (0.5 g·L^{-1}, MC16839), and metronidazole (0.25 g·L^{-1}, MB2200-1) [31], all of which were purchased from Meilunbio Biotech Co., Ltd. (Dalian, China). The successful establishment of the antibiotic-induced pseudo-germ-free model was confirmed by qPCR analysis of fecal samples, which showed a

marked reduction in bacterial DNA concentration.

2.7. Fecal microbiota transplantation (FMT)

Donor mouse feces (100 mg) were homogenized in 1 mL of sterile saline and centrifuged at 1000 r·min^{-1} for 3 min at 4 °C. A 100 μL aliquot of the supernatant containing bacteria was delivered to recipient mice *via* oral gavage [33]. Specifically, Stress + FMT group received daily FMT for 14 days after exposure to 14 days of chronic restraint stress, whereas sham-transplanted controls were given an equal volume (200 μL) of sterile PBS under identical conditions.

2.8. Preparation of G. elegans aqueous extract samples

Precisely 100 g of *G. elegans* powder was accurately weighed and immersed in 1000 mL of distilled water at room temperature overnight. The resulting suspension was then subjected to heat reflux extraction at 100 °C for 3 h. After cooling, the mixture was filtered through gauze to obtain a clear solution. The residue was extracted twice more under the same conditions for 2 h each. All three filtrates were combined, concentrated under reduced pressure with a rotary evaporator, and freeze-dried to yield a dry extract (extraction yield: 0.38% *W/W*, calculated as the weight of lyophilized extract relative to the initial dried material). The concentrations of major alkaloids in the aqueous extract were quantified by HPLC-MS/MS, revealing HMT, gelsemine, and koumine levels of 35.53, 15.8, and 53.46 μg·g^{-1}, respectively.

2.9. Toxicity assessment experiments

The dosages of *G. elegans* aqueous extract, gelsemine, and HMT were determined based on both pilot dose-response studies and previously reported LD_{50} values [11,12]. The aqueous extract was administered at 60 mg·kg^{-1}, as pilot studies indicated that a lower dose (30 mg·kg^{-1}) produced no detectable neurotoxicity, whereas a higher dose (120 mg·kg^{-1}) caused significant mortality. The intermediate dose (60 mg·kg^{-1}) consistently induced measurable neurotoxic effects without lethality (Figs. S1A and S1B), making it suitable for assessing disease-toxicity interactions. For the individual alkaloids, gelsemine and HMT were administered at 37.5 and 0.15 mg·kg^{-1}, respectively, corresponding to approximately 1/2 LD_{50} to LD_{50} based on literature-reported LD_{50} values. These doses were sufficient to induce neurotoxicity while avoiding mortality. Mice were euthanized 1 h post-administration, and blood and tissue samples were obtained. Brain levels of acetylcholine (ACh), acetylcholinesterase (AChE) and malondialdehyde (MDA) were quantified using commercial assay kits supplied by Jiancheng Bioengineering Institute (Nanjing, China). For the survival study, HMT was administered intraperitoneally at 0.2 mg·kg^{-1}, a dose slightly above its LD_{50}, and mouse mortality was monitored over 120 h following administration.

2.10. Clostridium scindens (C. scindens) culture and treatment

C. scindens (B295781; Ningbo Mingzhou Biotech Co., Ltd., Ningbo, China) was cultured anaerobically following the supplier's instructions. Bacterial cells were collected by centrifugation and resuspended in PBS. The resulting suspension was administered to experimental mice by oral gavage at a dose of 200 μL (1×10^9 CFU·mL^{-1}) once daily for 14 days [34]. The abundance of *C. scindens* in the mouse gut was measured by qPCR after bacterial colonization to assess the success of the colonization model.

2.11. Supplementation with lithocholic acid (LCA)

Intraperitoneal injections of LCA (31.25 mg·kg^{-1}) were given to mice once daily for four consecutive days following 24 days of restraint stress [35]. Subsequently, HMT toxicity experiments were conducted, and brain biochemical parameters were measured as previously described.

2.12. Real-time quantitative PCR analysis (qPCR)

Total RNA was isolated from tissues using RNAiso Plus reagent (Code No. 9180, Takara, Japan), while total DNA was extracted from cecal contents with a DNA extraction kit (FOREGENE, Chengdu, China). The integrity and concentration of RNA and DNA were determined according to protocols previously reported by our laboratory. For normalization, *16S rRNA* was used as the reference gene for DNA and *Gapdh* for RNA. The sequences of all primers used are presented in Table S1.

2.13. Western blotting

SDS-PAGE was performed to separate protein samples, followed by transfer onto PVDF membranes. The membranes were incubated with primary antibodies and then with secondary antibodies. Protein bands were visualized through enhanced chemiluminescence using the Omega LumG imaging system, and their intensities were quantified with ImageJ (version 1.8.0, NIH, USA). The primary antibodies used in this study included anti-CYP3A11 (A2544, ABclonal), PXR monoclonal antibody (67912-1-Ig, Proteintech), and anti-GAPDH (60004-1-Ig, Proteintech).

2.14. Liver microsome metabolism

Liver microsome metabolism assays were conducted as previously described [36]. Briefly, the incubation mixture comprised solution A, solution B, liver microsomes (0.5 mg·mL^{-1}), and testosterone (2 μg·mL^{-1}) in 50 mmol·L^{-1} potassium phosphate buffer. Samples were incubated for 1 h at 37 °C with shaking at 100 r·min^{-1}. Metabolism was terminated by adding three volumes of methanol, followed by centrifugation at 13 000 r·min^{-1} for 30 min at 4 °C. The supernatant was then collected for analysis using UPLC-MS/MS.

2.15. UPLC-MS/MS analysis

Liver and colon tissues were collected and homogenized in physiological saline at a 1∶10 (*W/V*) ratio. An ACQUITY^{TM} UPLC BEH C_{18} column (50 mm × 2.1 mm I.D., 1.7 μm) was used for chromatographic separation. Methanol (A) and water containing 0.1% formic acid (B) were used as the mobile phases. The elution program was as follows: 0–0.8 min, 5% A; 0.8–3.0 min, 5%–95% A; 3.0–3.5 min, 95% A; 3.5–4.0 min, 95%–5% A; 4.0–5.0 min, 5% A. Total flow rate was 0.3 mL·min^{-1}. *G. elegans* alkaloids, testosterone, and their metabolites were quantified by UPLC-MS/MS using the following MRM transitions: *m/z* 327.2→296.2 for HMT, *m/z* 323.2→236.2 for gelsemine, *m/z* 307.2→180.2 for koumine, *m/z* 343.2→312.3 for HMT metabolite, *m/z* 289.3→97.1 for testosterone, and *m/z* 305.3→269.3 for 6*β*-OH-testosterone. For the quantification of bile acids, the transitions of *m/z* 437→391 for CDCA, *m/z* 437→391 for UDCA, *m/z* 391→345.2 for DCA, *m/z* 421→375 for LCA, *m/z* 395→349.2 for the internal standard (IS, DCA-d_4) were performed.

2.16. 16S rRNA sequencing

Fecal bacterial DNA was isolated with the FastDNA^{TM} spin kit for soil (MP Biomedicals, Southern California, USA), and its concentration and purity were determined using a NanoDrop 2000 UV-Vis spectrophotometer [34]. The hypervariable region V3-V4 of the bacterial 16S rRNA gene was amplified using primer pairs

338F (5'-ACTCCTACGGGAGGCAGCAG-3') and 806R (5'-GGACTACHVGGGTWTCTAAT-3') on an ABI GeneAmp® 9700 PCR thermocycler. The PCR products were purified using the AxyPrep DNA gel extraction kit (Axygen Biosciences, CA, USA) according to the manufacturer's protocol and quantified with a Quantus™ Fluorometer (Promega, USA). Sequencing of the 16S rRNA amplicons was performed on the Illumina MiSeq platform (Majorbio Bio-pharm Technology Co., Ltd., Shanghai, China).

2.17. Shotgun metagenomics sequencing

For DNA obtained from control and stress mice, concentration was determined with a TBS-380, while purity was evaluated using a NanoDrop 2000 spectrophotometer. DNA extract was fragmented to an average size of about 400 bp using Covaris M220 (Gene Company Limited, China) for paired-end library construction. Paired-end library was constructed using NEXTFLEX Rapid DNA-Seq (Bioo Scientific, Austin, TX, USA). Paired-end sequencing was performed on Illumina Novaseq 6000 (Illumina Inc., San Diego, CA, USA) at Majorbio Bio-Pharm Technology Co., Ltd. (Shanghai, China) using NovaSeq 6000 S4 reagent kit according to the manufacturer's instructions (www.illumina.com). Open reading frames (ORFs) from each assembled contig were predicted using Prodigal, and ORFs with a length of ≥ 100 bp were retained. The best-hit taxonomy of non-redundant genes was assigned by aligning sequences against the NCBI NR database using DIAMOND with an e-value cutoff of 1×10^{-5}. To target the Kyoto Encyclopedia of Genes and Genomes database (http://www.genome.jp/kegg/), BLASTP (Version 2.2.28+) was utilized with an e-value cutoff of 1×10^{-5}.

2.18. GMrepo database analysis

Phenotypic associations based on genus-level relative microbial abundance were obtained from GMrepo, a comprehensive database of human gut metagenomic data [37]. This analysis served to provide supportive human evidence for the potential clinical relevance of the identified bacteria, rather than direct clinical validation of the animal model findings. After searching the database using the keyword "depression" (MeSH ID: D003863) to identify depression-associated samples, we performed a detailed screening process. We included only studies that reported shotgun metagenomic sequencing data from human stool samples with sufficient sequencing depth (excluding samples with less than 1 Gbp of quality reads) and comprehensive metadata distinguishing between healthy controls and clinically diagnosed depression patients. Samples were strictly excluded if the metadata indicated co-morbid major gastrointestinal diseases, history of antibiotic use within one month prior to sampling, or diagnosis of other severe psychiatric disorders (e.g., schizophrenia, bipolar disorder). The relative abundance of bacterial genera was calculated and normalized to 100% for each stool sample. Taxonomic annotation in the GMrepo database was performed centrally by the database curator using standardized metagenomic profilers (e.g., MetaPhlAn2). Using GMrepo RESTful APIs for R (version 3.6.1, https://www.r-project.org/) and the RStudio (version 1.1.442, https://posit.co/) software, genus-level abundance data for *Clostridium*, *Akkermansia*, and *Bifidobacterium* were retrieved from samples of both healthy individuals and patients with depression. Sample quality was evaluated by reviewing the associated metadata and supplementary materials from referenced publications. Subsequent analysis focused on comparing the relative abundance of *Clostridium* between the healthy and depressed groups, using the raw data provided by GMrepo without any modification or reprocessing of the original dataset.

2.19. Statistical analysis

Data are expressed as the mean ± standard error of the mean (SEM). Statistical comparisons between two groups were performed using Student's *t*-test, while comparisons among multiple groups were conducted using one-way or two-way ANOVA followed by Bonferroni's *post hoc* test to correct for multiple comparisons. The significance threshold was set at $P < 0.05$ after correction. In addition, all experimental data underwent rigorous quality control. Behavioral assessments were scored by two independent blinded experimenters with high inter-rater reliability. Molecular and omics data were subjected to standard quality checks (e.g., RNA integrity number > 8 for qPCR; sequencing depth > 10 000 reads per sample for 16S data). All statistical analyses were performed using GraphPad Prism 8 (GraphPad Software, USA). The specific statistical tests used are detailed in the figure legends.

3. Results

3.1. Depression significantly amplifies the neurotoxicity induced by *G. elegans* aqueous extract, gelsemine, or HMT

To investigate how depression influences the neurotoxicity induced by *G. elegans*, we first established a chronic restraint stress mouse model to mimic depression, a spared nerve injury (SNI) mouse model to simulate chronic neuropathic pain, and a combined mouse model to replicate the comorbidity of neuropathic pain and depression (Fig. 1A). Behavioral assessments showed that SNI and SNI + Stress mice exhibited a significant reduction in MWT, whereas SNI + Stress mice displayed markedly increased immobility in both the TST and FST, confirming successful establishment of the SNI and depression models (Figs. 1B and 1C). Notably, stress alone did not affect MWT (Figs. S2A and S2B). Under depressive conditions, the neurotoxicity of *G. elegans* aqueous extract, gelsemine, and HMT was significantly enhanced, as evidenced by elevated acetylcholine (ACh) and reduced acetylcholinesterase (AChE) activity (Figs. 1D–1F). In mice with comorbid depression and chronic pain, HMT administration induced pronounced neurotoxic effects, including increased brain ACh and malondialdehyde (MDA) levels, decreased AChE concentrations, and reduced survival rates. In contrast, under chronic pain alone, HMT toxicity remained unchanged (Figs. 1G and 1H). Collectively, these results demonstrate that depression, rather than chronic pain alone, plays a critical role in exacerbating *G. elegans* neurotoxicity.

3.2. Dysregulated gut microbiota amplifies HMT neurotoxicity in depressive states

To investigate the mechanisms underlying the heightened toxicity of HMT in depressive states, gut microbiota dysbiosis was first confirmed by 16S rRNA gene sequencing, revealing pronounced alterations in microbial diversity and composition (Figs. 2A and 2B). Next, the gut microbiota was depleted using a broad-spectrum antibiotic (Abx) cocktail, and qPCR analysis showed that Abx treatment markedly reduced fecal DNA concentrations, confirming successful microbiota depletion (Fig. S3A). Notably, Abx treatment alone did not alter key neurotoxicity markers in brain tissue, including ACh and AChE (Fig. S3B). Under HMT administration, however, Abx treatment abolished the depression-induced exacerbation of HMT neurotoxicity, as evidenced by the absence of significant differences in ACh, AChE, and MDA levels between the Abx-Control and Abx-Stress groups (Figs. 2C and 2D). These findings indicate that depletion of the gut microbiota masks the depression-induced exacerbation of HMT toxicity. To further validate the role of gut microbiota in HMT toxicity, FMT experiments were performed. Fecal microbiota from healthy donor mice was collected and transplanted into recipient mice

subjected to chronic stress (Fig. 2E). As expected, FMT significantly mitigated HMT neurotoxicity in stressed mice compared to stressed mice not receiving FMT (Fig. 2F). Collectively, these data indicate that the depression-induced increase in HMT toxicity is mediated, at least in part, through the gut microbiota.

3.3. Decreased abundance of Clostridium exacerbates HMT toxicity in depression

To elucidate how intestinal microbiota imbalance contributes to the exacerbation of HMT neurotoxicity under depressive conditions, we conducted 16S rRNA sequencing and shotgun metagenomic analysis to profile the gut microbiota of Control and Stress mice. The 16S rRNA sequencing identified 146 differential genera, while shotgun metagenomics revealed a broader spectrum of 1493 variable species (Fig. 3A). By integrating both datasets, we identified 78 genera that exhibited significant and concordant alterations in abundance (Fig. 3A). Pearson correlation analysis demonstrated strong agreement between the two datasets (Fig. 3B), and the abundance profiles of these 78 genera were visualized across both platforms (Figs. 3C and 3D). Among them, 52 genera showed consistent directional changes (Fig. 3E). To relate these findings to clinical relevance, we compared our data with the Data Repository for Human Gut Microbiota, which catalogs microbial signatures in healthy and depressed individuals. Notably, *Bifidobacterium*, *Akkermansia*, and *Clostridium* showed concordant trends in abundance across both species (Figs. 3F–3H). Cladogram and linear discriminant analysis (LDA) based on metagenomic data further pinpointed species-level changes: the relative abundances of *Bifidobacterium animalis*, *Akkermansia muciniphila*, *Clostridium* sp. CAG:452 and *Clostridia bacterium* were significantly reduced in Stress mice compared to Control mice (Figs. 3I–3K). Previous studies have reported that *Clostridium* constitutes approximately 10%–40% of the total human gut microbiota, whereas *Bifidobacterium* and *Akkermansia* typically account for less than 5% [38, 39]. Given that *Clostridium* sp. CAG:452, and *Clostridia bacterium* are not culturable or commercially available for *in vivo* studies, we selected *Clostridium scindens* (*C. scindens*), which possesses highly homologous bai gene clusters, to validate the functional role of *Clostridium* in HMT detoxification (Fig. 4A). Following successful colonization of stressed mice (Fig. S4A), HMT-induced neurotoxicity was markedly attenuated, as evidenced by significantly reduced brain levels of ACh and MDA, alongside restoration of AChE activity (Fig. 4B). Notably, colonization with *C. scindens* alone did not affect ACh or AChE levels in brain tissue (Fig. S4B). Further analysis showed that FMT increased the relative abundance of *C. scindens* in the feces of stressed mice (Fig. S4C). Collectively, these findings suggest that the depression-associated depletion of *Clostridium* plays a key role in mediating the heightened neurotoxicity of HMT. Restoration of *Clostridium* abundance may offer a promising strategy to mitigate herb-induced toxicity in depressive states.

3.4. Lower levels of LCA, a metabolite produced by Clostridium, exacerbate HMT toxicity in depression

To investigate how *Clostridium* mediates HMT toxicity in depression, we focused on its endogenous metabolic products. A major function of *Clostridium* involves bile acid metabolism, par-

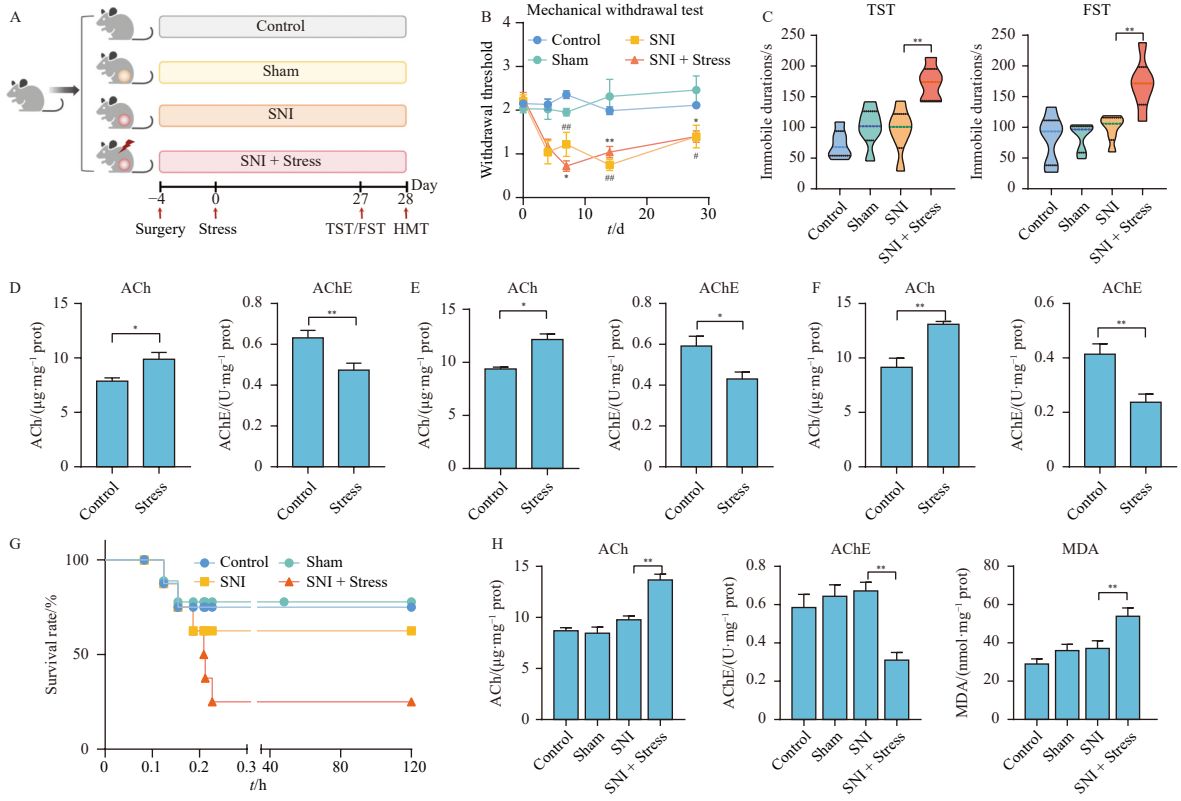

Fig. 1 Depression significantly amplifies the neurotoxicity induced by *G. elegans* aqueous extract, gelsemine, or HMT. (A) Schematic timeline of the experimental procedures involving spared nerve injury (SNI) combined with restraint stress and HMT toxicity assessment (0.15 mg·kg^{-1}, intraperitoneal injection). (B) The mechanical withdrawal test of Control, Sham, SNI, and SNI + Stress mice (n = 6 per group). (C) Immobility duration measured in TST and FST of Control, Sham, SNI, and SNI + Stress mice (n = 6 per group). (D) Brain tissue concentrations of acetylcholine (ACh) and acetylcholinesterase (AChE) after administration of *G. elegans* aqueous extract (n = 5 per group). (E) Brain tissue concentrations of ACh and AChE after administration of gelsemine (n = 5 per group). (F) Brain tissue concentrations of ACh and AChE after administration of HMT (n = 5 per group). (G) Survival rates of Control, Sham, SNI, and SNI + Stress mice following HMT administration (n = 9 per group). (H) Concentrations of ACh, AChE and malondialdehyde (MDA) in the brains of Control, Sham, SNI, and SNI + Stress mice (n = 5 per group). Data are presented as mean ± SEM. (D–F) were analyzed using Student's t-test, while (B, C, and H) were evaluated for statistical significance using one-way ANOVA with Bonferroni *post hoc* test. $^{\#}P < 0.05$, $^{\#\#}P < 0.01$, SNI *vs* Sham; $^{*}P < 0.05$, $^{**}P < 0.01$, SNI + Stress *vs* Sham.

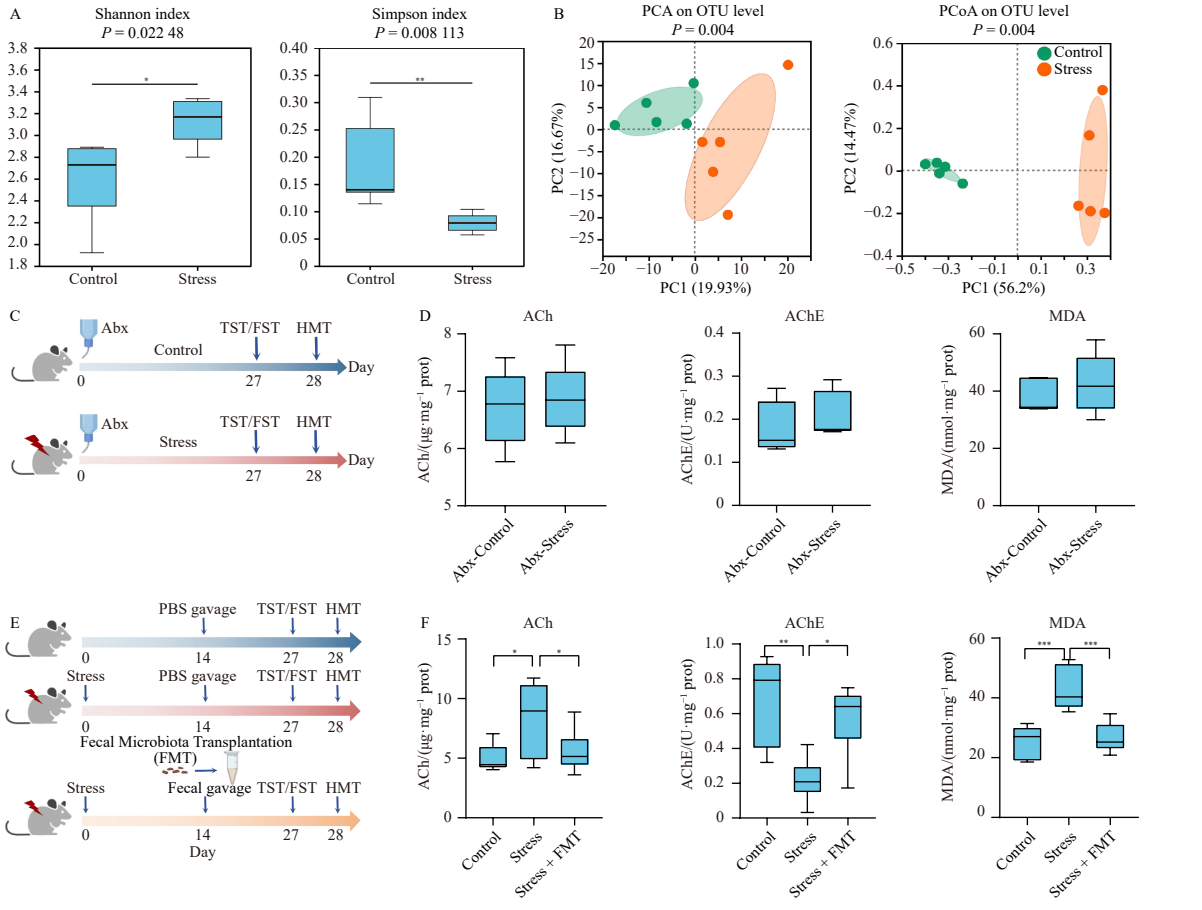

Fig. 2 Dysregulated gut microbiota amplifying HMT neurotoxicity during depression. (A) *α*-Diversity analysis using Shannon index and Simpson index at the operational taxonomic unit (OTU) level following 16S rRNA sequencing on fecal samples obtained from Control and Stress mice (n = 5 per group). (B) *β*-Diversity analysis using principal component analysis (PCA) and principal coordinates analysis (PCoA) on OTU level from Control and Stress mice (n = 5 per group). (C) Schematic timeline of restraint stress and HMT toxicity assessment in antibiotic-treated (Abx) mice. (D) Concentrations of ACh, AChE, and MDA in the brains of Abx-Control and Abx-Stress mice (n = 5 per group). (E) Schematic timeline of restraint stress, fecal microbiota transplantation (FMT), and HMT toxicity assessment experiments. (F) Concentrations of ACh, AChE, and MDA in the brains of Control, Stress, and Stress + FMT mice (n = 6 per group). Data are presented as mean ± SEM. (D) was analyzed using Student's t-test (*vs* Abx-Control group). while (F) was evaluated for statistical significance using one-way ANOVA with Bonferroni *post hoc* test (*vs* Stress group). $^{*}P < 0.05$, $^{**}P < 0.01$, $^{***}P < 0.001$.

ticularly the conversion of primary bile acids into secondary bile acids. One notable pathway (Fig. 4C) involves the transformation of chenodeoxycholic acid (CDCA) into ursodeoxycholic acid (UDCA), followed by further metabolism into LCA and deoxycholic acid (DCA) *via* the 7*α*-dehydroxylation pathway by *Clostridium* [40]. In our study, significant differences in total bile acid content were observed in both the liver (Fig. 4D) and colon (Fig. 4E) between Stress and Control mice. Targeted metabolomics revealed that stressed mice exhibited markedly lower LCA levels in both the liver and colon compared with controls, whereas UDCA levels were elevated. Additionally, CDCA levels in the liver increased, while DCA decreased in stressed mice (Fig. 4F). Since bile acid-inducible enzymes, such as *baiCD*, play a rate-limiting role in converting CDCA and UDCA into LCA and DCA [41], we performed PCR experiments targeting the specific gene encoding the 7*α*-dehydroxylation enzyme. These experiments revealed significant downregulation of *baiCD* gene expression in the gut microbiota of stressed mice (Fig. 4G). This suggests that depression-induced alterations in gut microbiota composition impair the microbial metabolism of bile acids, leading to reduced LCA and DCA production.

To assess the functional role of LCA, mice were supplemented with a non-hepatotoxic dose of 31.25 mg·kg^{-1} LCA (Fig. S4D). LCA treatment alone did not alter brain ACh and AChE levels (Fig. S4E). However, in stressed mice receiving HMT, LCA significantly reduced brain ACh and MDA levels while restoring AChE activity (Figs. 4H and 4I). These findings demonstrate that lower levels of LCA, a metabolite produced by *Clostridium*, contribute to the exacerbation of HMT neurotoxicity under depressive conditions, and that LCA supplementation can mitigate this effect.

3.5. Reduced LCA levels suppress the PXR-CYP3A11 axis, exacerbating HMT toxicity in depressive states

LCA has been reported as a ligand of PXR, a nuclear receptor that regulates metabolic enzyme activity [42]. In wild-type mice, hepatic PXR mRNA and protein expression were reduced under depression but restored following LCA supplementation (Fig. 5A). In contrast, in *Pxr* knockout ($Pxr^{-/-}$) mice, LCA supplementation had no effect on ACh, AChE, or MDA levels, indicating that the protective effects of LCA are PXR-dependent (Figs. 5B and 5C). Importantly, under depression, no significant changes were observed in the expression of other nuclear receptors, including constitutive CAR, farnesoid X receptor (FXR), peroxisome proliferator-activated receptor-α (PPAR-α), and aryl hydrocarbon receptor (AHR) (Figs. 5D–5F). Moreover, in stressed mice with gut microbiota depletion, the *Clostridium*-LCA axis was no longer functional, and PXR expression remained unchanged (Fig. 5G). Restoration of the axis *via* fecal microbiota transplantation or *C. scindens* colonization significantly upregulated PXR expression (Figs. 5H and 5I). These findings suggest that LCA depletion under depressive conditions contributes to enhanced HMT neurotoxicity by downregulating PXR expression.

CYP3A11, a key PXR-regulated metabolic enzyme, detoxifies HMT by converting it into less toxic metabolites [43]. Under depressive conditions, CYP3A11 expression at both the gene

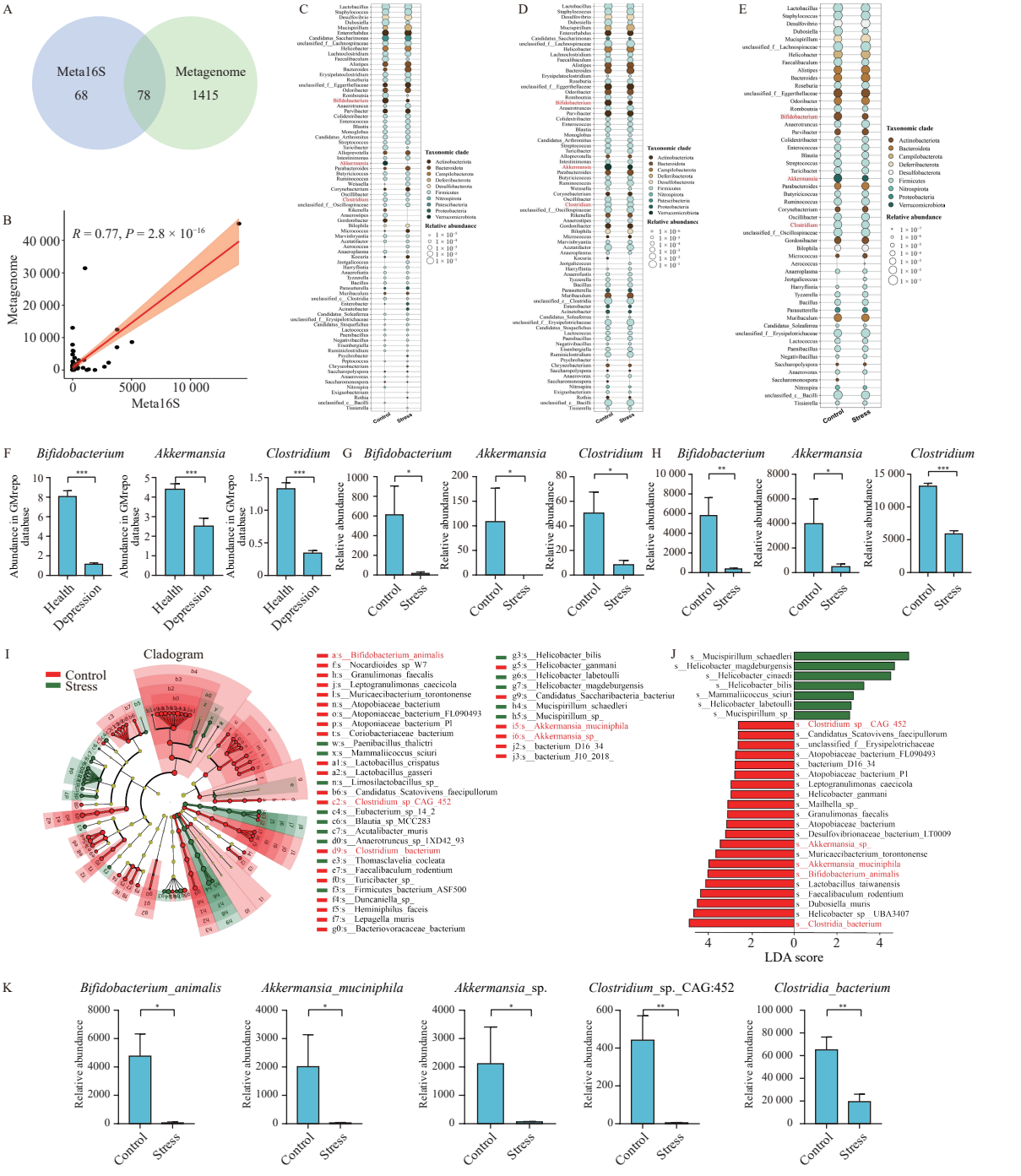

Fig. 3 The abundance of *Clostridium* is significantly reduced in both stressed mice and patients with depression. (A) Venn diagram illustrates the number of shared bacterial genera identified in fecal samples from Control and Stress mice through both 16S rRNA sequencing and shotgun metagenomic. (B) Pearson's correlation of shared genus observed between 16S rRNA sequencing and shotgun metagenomics ($R = 0.77$; $P = 2.8 \times 10^{-16}$). Bubble chart showing the relative abundance of the shared genera identified by 16S rRNA sequencing (C) and shotgun metagenomics (D). (E) Bubble chart illustrating the relative abundance of shared genera that exhibit consistent variation in shotgun metagenomics. (F) The fecal abundance of *Bifidobacterium*, *Clostridium* and *Akkermansia* in healthy individuals ($n = 1000$) and patients with depression ($n = 351$) from GMrepo database. 16S rRNA sequencing (G) and Shotgun metagenomics (H) analysis showing the relative abundance of *Bifidobacterium*, *Clostridium* and *Akkermansia* in fecal samples from Control and Stress mice. (I) Cladogram depicting differentially abundant taxa between Control and Stress mice base on shotgun metagenomics. (J) Linear discriminant analysis (LDA) effect size (LEfSe) was used to analyze the differentially abundant taxa between Control and Stress mice in the shotgun metagenomics, and displayed as a histogram (LDA score > 2.2, $P < 0.01$). (K) Shotgun metagenomics showing the abundance of *Bifidobacterium_animalis*, *Akkermansia_muciniphila*, *Akkermansia*_sp., *Clostridium*_sp._CAG:452, and *Clostridium_bacterium* in fecal samples from Control and Stress mice. Control and Stress mice ($n = 5$ per group) applied consistently across all panels (C–E, G–K). Data are presented as mean ± SEM. Statistical significance was assessed using *t*-test. $^{*}P < 0.05$, $^{**}P < 0.01$, $^{***}P < 0.001$. (F) *vs* Health group; (G, H, K) *vs* Control group.

(Figs. 6A and 6B) and protein (Figs. 6C and 6D) levels, as well as its enzymatic activity (Fig. S5A), was significantly reduced. Correspondingly, HMT levels increased by 2.69-fold, while its less toxic metabolites decreased by 50% (Figs. 6E and S5B). In $Pxr^{-/-}$ mice, CYP3A11 expression (Figs. 6F and 6G) and HMT toxicity (Figs. S6A–S6C) remained unchanged under depressive conditions. Further experiments demonstrated that CYP3A11 expression was significantly upregulated following FMT (Fig. 6H), *C. scindens* colonization (Fig. 6I), or LCA supplementation (Fig. 6J), coinciding with reduced HMT neurotoxicity. Together, these findings indicate that depression-associated reduction of LCA suppresses the PXR-CYP3A11 axis, leading to heightened HMT toxicity, whereas LCA supplementation restores this axis and mitigates toxicity.

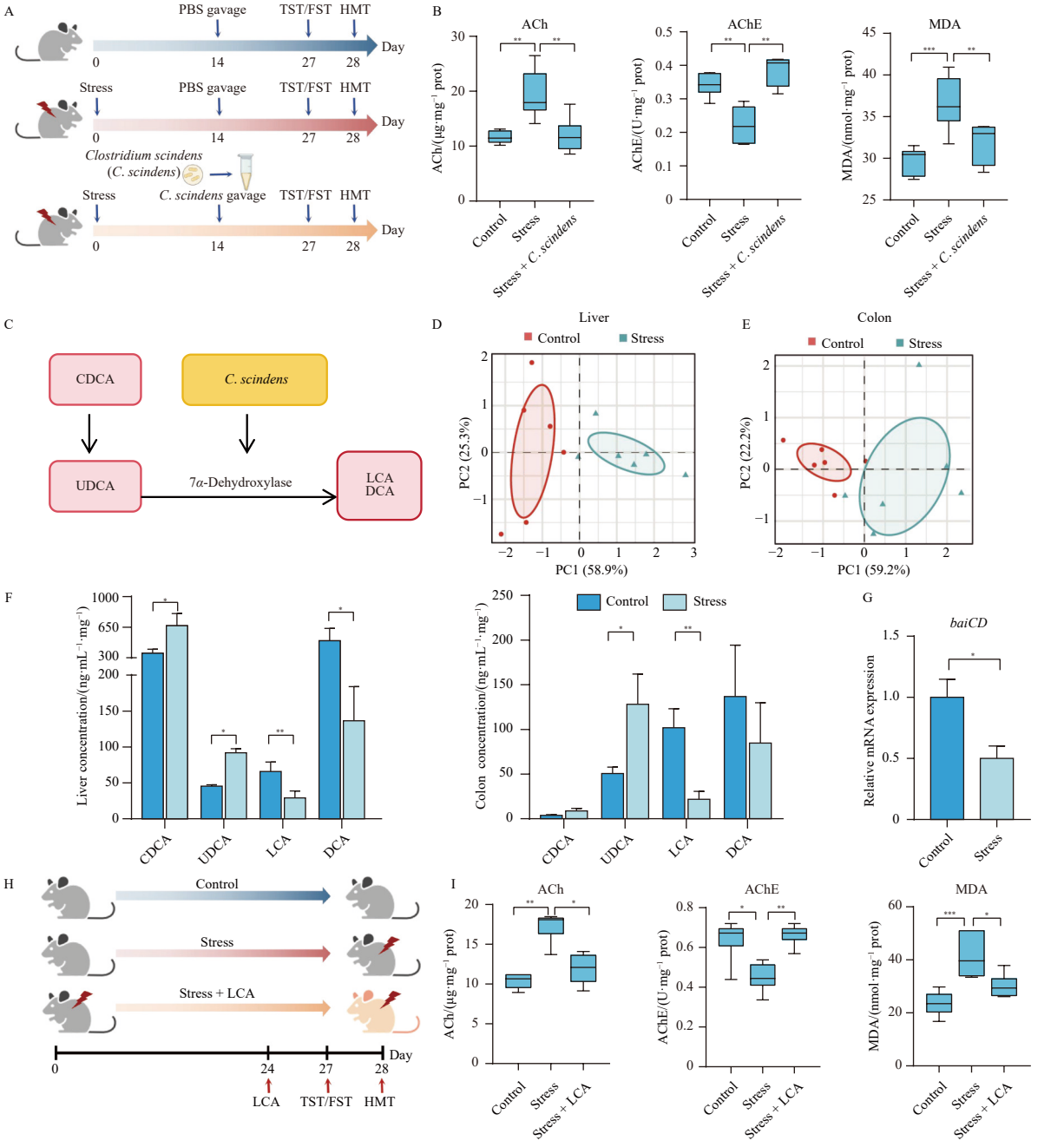

Fig. 4 Supplementation with *Clostridium scindens* (*C. scindens*) or its metabolite lithocholic acid (LCA) reduces HMT neurontoxicity under depression. (A) Schematic timeline of restraint stress, *C. scindens* colonization, and HMT toxicity assessment experiments. (B) Concentrations of ACh, AChE, and MDA in the brains of Control, Stress, and Stress + *C. scindens* mice (n = 6 per group). (C) Schematic diagram illustrating the conversion of primary bile acids to secondary bile acids *via* 7α-dehydroxylase in the intestines. PCA score scatter based on liver (D) and colon (E) total bile acid concentrations by metabolomic analyses of Control and Stress mice (n = 6 per group). (F) Concentrations of chenodeoxycholic acid (CDCA), ursodeoxycholic acid (UDCA), LCA and deoxycholic acid (DCA) in the liver and colon (n = 6 per group). (G) The mRNA expression of *baiCD* (the specific encoding gene of 7α-dehydroxylase) in Control and Stress mice (n = 6 per group). (H) Schematic timeline of restraint stress, LCA supplementation, and HMT toxicity assessment experiments. (I) Concentrations of ACh, AChE, and MDA in the brains of Control, Stress, and Stress + LCA mice (n = 6 per group). Data are presented as mean ± SEM. (F and G) were analyzed by Student's t-test (*vs* Control group). Data in (B and I) were evaluated by one-way ANOVA with Bonferroni *post hoc* test (*vs* Stress group). $^{*}P < 0.05$, $^{**}P < 0.01$, $^{***}P < 0.001$.

4. Discussion

This study provides novel mechanistic evidence that comorbid depression significantly exacerbates the neurotoxicity of *G. elegans* and its major indole alkaloids, gelsemine, and HMT *via* disruption of a gut microbiota-host metabolic axis. Specifically, we identified a depression-induced impairment of the *Clostridium*-LCA-PXR-CYP3A11 pathway, a key hepatic detoxification route for indole alkaloids. These findings not only reveal a previously unrecognized mechanism underlying disease-modified toxicity of traditional herbal medicines. They also underscore the potential of gut microbial modulation to mitigate toxicity risks.

The ethnomedical use of *G. elegans* to treat chronic pain, particularly in Southeast Asia, has long been shadowed by its potent neurotoxicity [1]. Our findings suggest that this risk may be further amplified in individuals with depression, a common comorbidity of chronic pain. Building on prior reports that depression can alter drug metabolism and herb safety, our study directly links depression-associated microbial dysbiosis to a bile acid-nuclear receptor signaling defect that governs detoxification of *G. elegans* alkaloids.

Depression has been widely shown to disrupt gut microbial homeostasis [44]. Gut microbiota and their metabolites play central roles in modulating drug metabolism and toxicity. In this study,

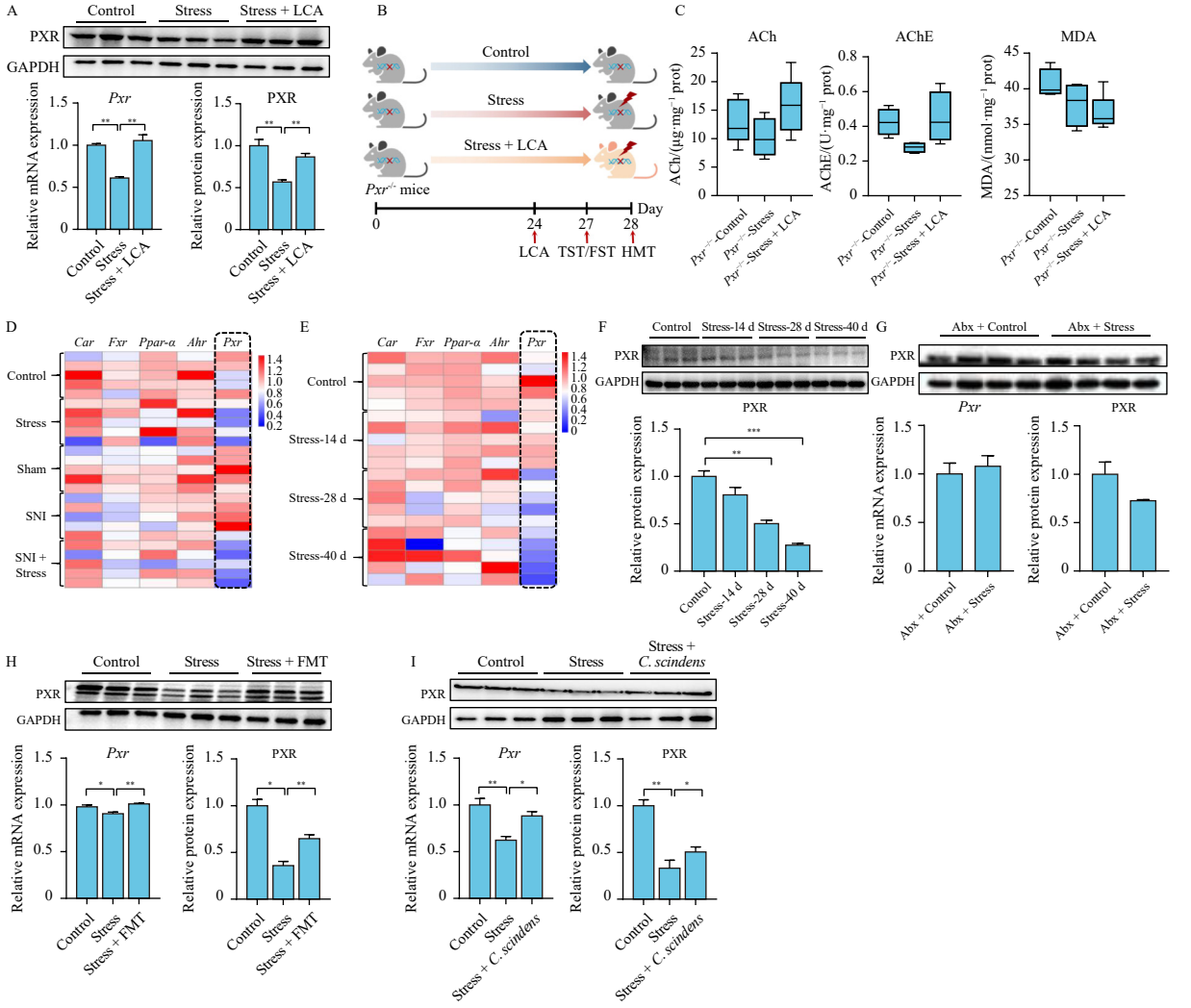

Fig. 5 In depressive states, LCA restores PXR activation to mitigate HMT neurotoxicity. (A) Relative expression of liver *Pxr* mRNA (n = 6 per group) and PXR protein (n = 3 per group) in Control, Stress, and Stress + LCA mice. (B) Schematic timeline of restraint stress, LCA supplementation, and HMT toxicity assessment experiments in *Pxr* knockout ($Pxr^{-/-}$) mice. (C) Concentrations of ACh, AChE, and MDA in the brains of $Pxr^{-/-}$-Control, $Pxr^{-/-}$-Stress, and $Pxr^{-/-}$-Stress + LCA mice (n = 6 per group). (D) Hepatic mRNA expression of nuclear receptors *Pxr*, *Car*, *Fxr*, *Ppar-α*, and *Ahr* in Control, Sham, SNI, Stress, and SNI + Stress mice (n = 5 per group). (E) Hepatic mRNA expression of nuclear receptors *Pxr*, *Car*, *Fxr*, *Ppar-α*, and *Ahr* in Control and different stages of Stress mice (n = 5 per group). (F) Hepatic protein expression of PXR in Control and different stages of Stress mice (n = 3 per group). (G) Relative expression of liver *Pxr* mRNA (n = 6 per group) and PXR protein (n = 4 per group) expression in Abx-Control and Abx-Stress mice. (H) Relative expression of liver *Pxr* mRNA (n = 6 per group) and PXR protein (n = 3 per group) expression in Control, Stress, and Stress + FMT mice. (I) Relative expression of liver *Pxr* mRNA (n = 6 per group) and PXR protein (n = 3 per group) expression in Control, Stress, and Stress + *C. scindens* mice. Data are presented as mean ± SEM. (G) was analyzed using Student's *t*-test (*vs* Control group). (F) was compared to the Control group, and (A, C, H, and I) were compared to the Stress group; these five panels were evaluated for statistical significance using one-way ANOVA with Bonferroni *post hoc* test. $^{*}P < 0.05$, $^{**}P < 0.01$, $^{***}P < 0.001$.

depression markedly reduced the abundance of *Clostridium*, with *Clostridium* sp. CAG:452 and *Clostridia bacterium* showing the most significant decreases. These taxa lack available reference strains, but literature indicates high sequence similarity with *C. scindens*, which harbors a highly conserved *bai* gene cluster encoding 7*α*-dehydroxylase, which converts primary bile acids into secondary bile acids, such as DCA and LCA [41, 45, 46]. Colonization with *C. scindens* significantly mitigated depression-exacerbated HMT neurotoxicity, confirming its pivotal role in this mechanism.

LCA, a major metabolite of *C. scindens*, exhibits multiple pharmacological activities, including anti-aging and immune modulation [47, 48]. However, excessive LCA induces hepatotoxicity and promotes carcinogenesis [49]. Our study identified 31.25 mg·kg^{-1} as a relatively safe and effective dose of LCA, which effectively reversed the depression-exacerbated HMT neurotoxicity. Notably, plasma LCA concentrations in mice (about 50–500 nmol·L^{-1}) are substantially higher than those in humans (about 10–30 nmol·L^{-1}) [50, 51], indicating that further studies are needed to extrapolate effective doses from animals to clinical settings.

Mechanistically, our data indicate that depressive conditions selectively suppress the PXR-CYP3A11 detoxification axis while leaving other nuclear receptors (FXR, CAR, PPAR-α, and AHR) largely unchanged. This selectivity is consistent with ligand-dependent regulation: LCA is an established endogenous agonist of PXR and potently enhances PXR expression and activity [52], whereas FXR, CAR, PPAR-α and AHR are activated by distinct ligands (e.g., CDCA and other primary bile acids for FXR; xenobiotics or certain steroids for CAR; fatty acids for PPAR-α; planar aromatic compounds for AHR) [53-56]. Therefore, depression appears to disrupt a highly specific microbiota-LCA-PXR axis rather than inducing broad dysregulation across nuclear receptor networks. This mechanistic selectivity underscores the pivotal role of PXR in mediating the comorbidity-dependent enhancement of HMT neurotoxicity.

Our previous study demonstrated that HMT detoxification depends on CYP3A11-mediated metabolism [57]. Stress disrupted the *Clostridium*-LCA-PXR-CYP3A11 axis, suppressing HMT metabolism and leading to accumulation of parent compounds and exacerbated neurotoxicity. Restoration of this axis *via C. scindens* colonization, LCA supplementation, or FMT markedly alleviated HMT-induced toxicity, emphasizing the key role of host-microbiota co-metabolism. CYP3A11, the murine ortholog of human

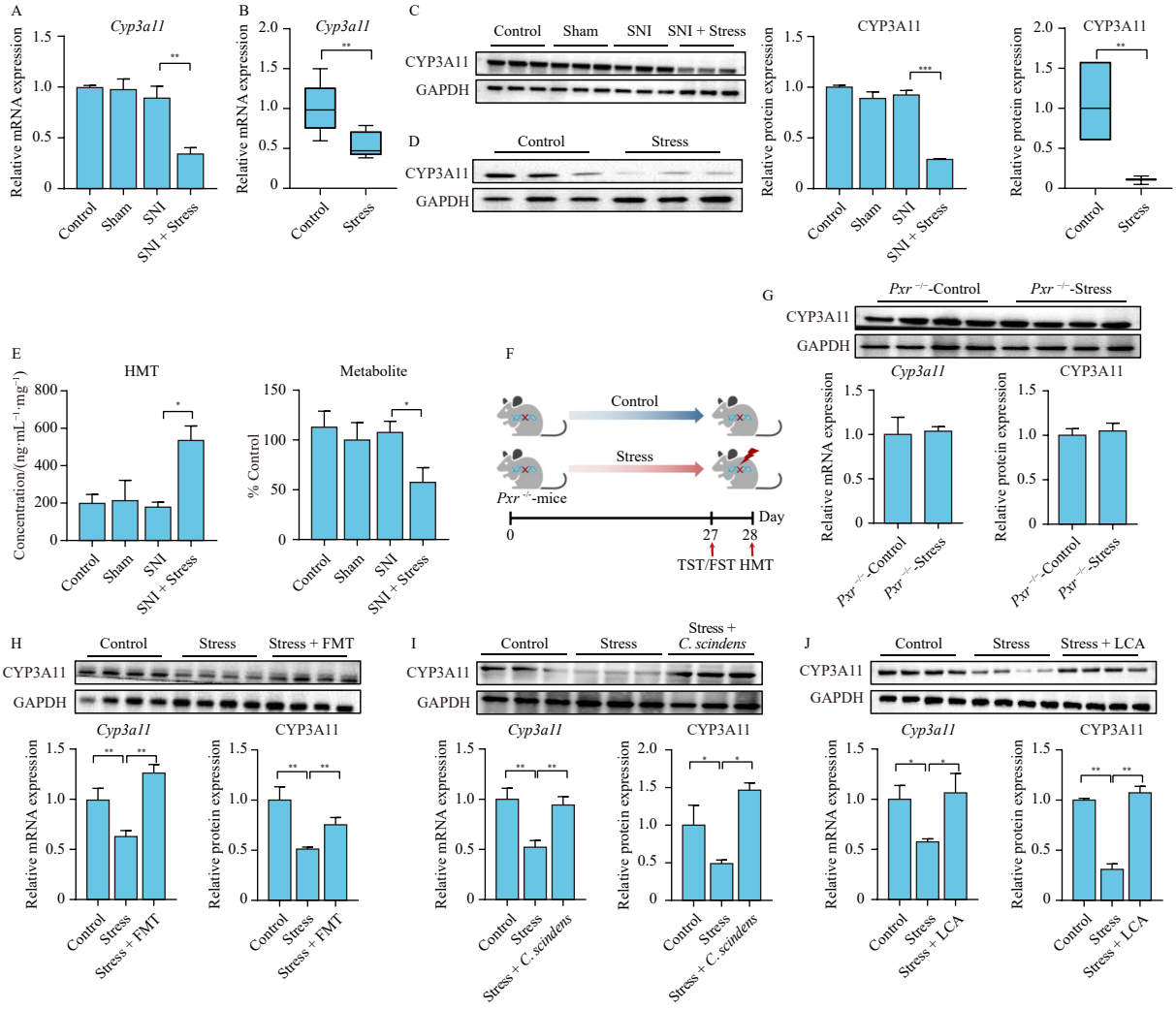

Fig. 6 PXR-driven upregulation of CYP3A11 alleviates HMT neurotoxicity under depressive conditions. (A) The mRNA expression of *Cyp3a11* in Control, Sham, SNI, and SNI + Stress mice (n = 5 per group). (B) The mRNA expression of *Cyp3a11* in Control and Stress mice (n = 5 per group). (C) The protein expression of CYP3A11 in Control, Sham, SNI, and SNI + Stress mice (n = 3 per group). (D) The protein expression of CYP3A11 in Control and Stress mice (n = 3 per group). (E) Concentrations of HMT and HMT-hydroxylation metabolite in the liver of Control, Sham, SNI, and SNI + Stress mice (n = 5 per group). (F) Schematic timeline of the experimental procedures involving restraint stress and HMT toxicity assessment in *Pxr*$^{-/-}$ mice. (G) Relative expression of liver *Cyp3a11* mRNA and CYP3A11 protein in *Pxr*$^{-/-}$-Control and *Pxr*$^{-/-}$-Stress mice (n = 4 per group). (H) Relative expression of liver *Cyp3a11* mRNA (n = 6 per group) and CYP3A11 protein (n = 4 per group) in Control, Stress, and Stress + FMT mice. (I) Relative expression of liver *Cyp3a11* mRNA (n = 6 per group) and CYP3A11 protein (n = 3 per group) in Control, Stress, and Stress + *C. scindens* mice. (J) Relative expression of liver *Cyp3a11* mRNA (n = 6 per group) and CYP3A11 protein (n = 4 per group) in Control, Stress, and Stress + LCA mice. Data are presented as mean ± SEM. (B, D, and G) were analyzed using Student's t-test (*vs* Control group). Statistical significance for (A, C, E) (*vs* SNI group) and (H, I, J) was evaluated using one-way ANOVA with Bonferroni *post hoc* test. $^{*}P < 0.05$, $^{**}P < 0.01$, $^{***}P < 0.001$.

CYP3A4, is a key hepatic enzyme responsible for the metabolism of a broad spectrum of xenobiotics, including midazolam, simvastatin, and cyclosporine A [58-60], as well as natural products such as ginsenosides from *Panax ginseng* and curcumin from *Curcuma longa* [61, 62]. Thus, the *C. scindens*-LCA-PXR-CYP3A11 axis identified here may represent a broader mechanism through which depression modulates the metabolism of drugs and herbal compounds, extending beyond HMT detoxification. Notably, although SNI has been reported to alter gut microbial composition [63, 64], our data show that it does not aggravate HMT-induced neurotoxicity because the *C. scindens*-LCA-PXR-CYP3A11 signaling axis remains intact.

Beyond *Clostridium*, reductions in other beneficial taxa, such as *Akkermansia* and *Bifidobacterium*, known for their roles in modulating bile acid profiles and ameliorating depressive-like behaviors [23, 65, 66], though their contribution to alkaloid detoxification remains to be clarified.

5. Conclusions

Taken together, our study reveals that depression-driven disruption of the *Clostridium*-LCA-PXR-CYP3A11 axis impairs the detoxification of *G. elegans* alkaloids, exacerbating neurotoxicity. This highlights a critical link between psychiatric conditions, gut microbiota, and herbal medicine safety. Microbiota-based interventions, including probiotics or bile acid modulation, may offer promising strategies to reduce toxicity and support safer, individualized use of plant-based remedies.

Funding

This work was supported by the National Natural Science Foundation of China (Nos. 82422077 and 82274193) and Guangdong Basic and Applied Basic Research Foundation (No. 2024B1515020093).

Data availability statement

The 16S rRNA and shotgun metagenomics sequencing datasets are available in the NCBI SRA database under the accession numbers PRJNA1073719 and PRJNA1077725, respectively. Supporting information for this study can be obtained by con-

tacting the corresponding authors *via* E-mail.

Acknowledgments

The *Pxr* knockout mice utilized in this study were generously provided by Prof. Fei Li (Sichuan University).

Declarations

The authors have declared that no conflict of interest exist.

References

1 Huang CY, Zuo MT, Qi XJ, et al. Hypoxia tolerance determine differential gelsenicine-induced neurotoxicity between pig and mouse. *BMC Med*. 2025; 23(1):156. https://doi.org/10.1186/s12916-025-03984-5.
2 Liu Y, Tang Q, Cheng P, et al. Whole-genome sequencing and analysis of the Chinese herbal plant *Gelsemium elegans*. *Acta Pharm Sin B*. 2020;10(2):374-382. https://doi.org/10.1016/j.apsb.2019.08.004.
3 Li Y, Hu P, Zhang Z, et al. Protective autophagy alleviates neurotoxin-gelsenicine induced apoptosis through PERK signaling pathway in Neuro-2a cells. *Toxicology*. 2022;474:153210. https://doi.org/10.1016/j.tox.2022.153210.
4 Liu D, Liu Y, Shen A, et al. Analysis of alkaloids in *Gelsemium elegans* Benth using an online heart-cutting + comprehensive RPLC × RPLC system tandem mass spectrometry. *Talanta*. 2022;239:123069. https://doi.org/10.1016/j.talanta.2021.123069.
5 Jin GL, Su YP, Liu M, et al. Medicinal plants of the genus *Gelsemium* (gelsemiaceae, gentianales): a review of their phytochemistry, pharmacology, toxicology and traditional use. *J Ethnopharmacol*. 2014;152(1):33-52. https://doi.org/10.1016/j.jep.2014.01.003.
6 Wu YE, Li YD, Luo YJ, et al. Gelsemine alleviates both neuropathic pain and sleep disturbance in partial sciatic nerve ligation mice. *Acta Pharmacol Sin*. 2015;36(11):1308-1317. https://doi.org/10.1038/aps.2015.86.
7 Zhang JY, Wang YX. *Gelsemium* analgesia and the spinal glycine receptor/allopregnanolone pathway. *Fitoterapia*. 2015;100:35-43. https://doi.org/10.1016/j.fitote.2014.11.002.
8 Liu D, Wang JX, Hou T, et al. Dihydrokoumine, a dual-target analgesic with reduced side effects isolated from a traditional Chinese medicine. *J Adv Res*. 2024;74:637-649. https://doi.org/10.1016/j.jare.2024.10.011.
9 Lin HL, Qiu HQ, Cheng Y, et al. *Gelsemium elegans* Benth: chemical components, pharmacological effects, and toxicity mechanisms. *Molecules*. 2021;26(23):7145. https://doi.org/10.3390/molecules26237145.
10 Ma X, Wang ZY, Zuo MT, et al. Excretion, metabolism, and tissue distribution of *Gelsemium elegans* (*Gardn. & Champ.*) Benth in pigs. *Molecules*. 2022;27(8): 2605. https://doi.org/10.3390/molecules27082605.
11 Rujjanawate C, Kanjanapothi D, Panthong A. Pharmacological effect and toxicity of alkaloids from *Gelsemium elegans* Benth. *J Ethnopharmacol*. 2003;89(1):91-95. https://doi.org/10.1016/s0378-8741(03)00267-8.
12 Long JY, Wang ZY, Zuo MT, et al. Effect of cytochrome P450 3A4 on tissue distribution of humantenmine, koumine, and gelsemine, three alkaloids from the toxic plant *Gelsemium*. *Toxicol Lett*. 2024;397:34-41. https://doi.org/10.1016/j.toxlet.2024.05.002.
13 Lee MT, Peng WH, Wu CC, et al. Impaired ventrolateral periaqueductal gray-ventral tegmental area pathway contributes to chronic pain-induced depression-like behavior in mice. *Mol Neurobiol*. 2023;60(10):5708-5724. https://doi.org/10.1007/s12035-023-03439-z.
14 Bair MJ, Robinson RL, Katon W, et al. Depression and pain comorbidity: a literature review. *Arch Intern Med*. 2003;163(20):2433-2445. https://doi.org/10.1001/archinte.163.20.2433.
15 Ganey PE, Luyendyk JP, Maddox JF, et al. Adverse hepatic drug reactions: inflammatory episodes as consequence and contributor. *Chem Biol Interact*. 2004;150(1):35-51. https://doi.org/10.1016/j.cbi.2004.09.002.
16 Russo M, Della SA, Tocchetti CG, et al. Metabolic aspects of anthracycline cardiotoxicity. *Curr Treat Options Oncol*. 2021;22(2):18. https://doi.org/10.1007/s11864-020-00812-1.
17 Liu Y, Wang W, Sun M, et al. Polygonum multiflorum-induced liver injury: clinical characteristics, risk factors, material basis, action mechanism and current challenges. *Front Pharmacol*. 2019;10:1467. https://doi.org/10.3389/fphar.2019.01467.
18 Sun S, Zhu L, Hu Y, et al. Studies on the metabolism of paeoniflorin in human intestinal microflora by high performance liquid chromatography/electrospray ionization/Fourier transform ion cyclotron resonance mass spectrometry and quadrupole time-of-flight mass spectrometry. *J Chromatogr B Analyt Technol Biomed Life Sci*. 2018;1085:63-71. https://doi.org/10.1016/j.jchromb.2018.03.042.
19 Fung TC, Vuong HE, Luna CDG, et al. Intestinal serotonin and fluoxetine exposure modulate bacterial colonization in the gut. *Nat Microbiol*. 2019;4 (12):2064-2073. https://doi.org/10.1038/s41564-019-0540-4.
20 Zheng P, Zeng B, Zhou C, et al. Gut microbiome remodeling induces depressive-like behaviors through a pathway mediated by the host's metabolism. *Mol Psychiatry*. 2016;21(6):786-796. https://doi.org/10.1038/mp.2016.44.
21 Qu W, Liu S, Zhang W, et al. Impact of traditional Chinese medicine treatment on chronic unpredictable mild stress-induced depression-like behaviors: intestinal microbiota and gut microbiome function. *Food Funct*. 2019;10(9): 5886-5897. https://doi.org/10.1039/c9fo00399a.
22 Cryan JF, Dinan TG. Mind-altering microorganisms: the impact of the gut microbiota on brain and behaviour. *Nat Rev Neurosci*. 2012;13(10):701-712. https://doi.org/10.1038/nrn3346.
23 Dempsey JL, Cui JY. Microbiome is a functional modifier of P450 drug metabolism. *Curr Pharmacol Rep*. 2019;5(6):481-490. https://doi.org/10.1007/s40495-019-00200-w.
24 Tsunoda SM, Gonzales C, Jarmusch AK, et al. Contribution of the gut microbiome to drug disposition, pharmacokinetic and pharmacodynamic variability. *Clin Pharmacokinet*. 2021;60(8):971-984. https://doi.org/10.1007/s40262-021-01032-y.
25 Gao Y, Lin J, Ye C, et al. Microbial transformations of bile acids and their receptors in the regulation of metabolic dysfunction-associated steatotic liver disease. *Liver Res*. 2023;7(3):165-176. https://doi.org/10.1016/j.livres.2023.09.002.
26 Masse KE, Lu VB. Short-chain fatty acids, secondary bile acids and indoles: gut microbial metabolites with effects on enteroendocrine cell function and their potential as therapies for metabolic disease. *Front Endocrinol (Lausanne)*. 2023;14:1169624. https://doi.org/10.3389/fendo.2023.1169624.
27 Liu L, Wang H, Chen X, et al. Gut microbiota and its metabolites in depression: from pathogenesis to treatment. *EBioMedicine*. 2023;90:104527. https://doi.org/10.1016/j.ebiom.2023.104527.
28 Zhang T, Rao Q, Dai M, et al. *Tripterygium wilfordii* protects against an animal model of autoimmune hepatitis. *J Ethnopharmacol*. 2023;309:116365. https://doi.org/10.1016/j.jep.2023.116365.
29 Hu X, Du L, Liu S, et al. A TRPV4-dependent neuroimmune axis in the spinal cord promotes neuropathic pain. J Clin Invest. 2023;133(5):e161507. https://doi.org/10.1172/JCI161507.
30 Dellarole A, Morton P, Brambilla R, et al. Neuropathic pain-induced depressive-like behavior and hippocampal neurogenesis and plasticity are dependent on TNFR1 signaling. *Brain Behav Immun*. 2014;41:65-81. https://doi.org/10.1016/j.bbi.2014.04.003.
31 Ye L, Hou Y, Hu W, et al. Repressed *Blautia*-acetate immunological axis underlies breast cancer progression promoted by chronic stress. *Nat Commun*. 2023;14(1):6160. https://doi.org/10.1038/s41467-023-41817-2.
32 Gao X, Cao Q, Cheng Y, et al. Chronic stress promotes colitis by disturbing the gut microbiota and triggering immune system response. *Proc Natl Acad Sci U S A*. 2018;115(13):E2960-E2969. https://doi.org/10.1073/pnas.1720696115.
33 Zhao Z, Ning J, Bao XQ, et al. Fecal microbiota transplantation protects rotenone-induced Parkinson's disease mice *via* suppressing inflammation mediated by the lipopolysaccharide-TLR4 signaling pathway through the microbiota-gut-brain axis. *Microbiome*. 2021;9(1):226. https://doi.org/10.1186/s40168-021-01107-9.
34 Tang D, Hu W, Fu B, et al. Gut microbiota-mediated C-sulfonate metabolism impairs the bioavailability and anti-cholestatic efficacy of andrographolide. *Gut Microbes*. 2024;16(1):2387402. https://doi.org/10.1080/19490976.2024.2387402.
35 Lajczak-McGinley NK, Porru E, Fallon CM, et al. The secondary bile acids, ursodeoxycholic acid and lithocholic acid, protect against intestinal inflammation by inhibition of epithelial apoptosis. *Physiol Rep*. 2020;8(12): e14456. https://doi.org/10.14814/phy2.14456.
36 Wang Z, Lan Y, Chen M, et al. Eriodictyol, not its glucuronide metabolites, attenuates acetaminophen-induced hepatotoxicity. *Mol Pharm*. 2017;14(9): 2937-2951. https://doi.org/10.1021/acs.molpharmaceut.7b00345.
37 Wu S, Sun C, Li Y, et al. GMrepo: a database of curated and consistently annotated human gut metagenomes. *Nucleic Acids Res*. 2020;48(D1):D545-D553. https://doi.org/10.1093/nar/gkz764.
38 Lopetuso LR, Scaldaferri F, Petito V, et al. Commensal *Clostridia*: leading players in the maintenance of gut homeostasis. *Gut Pathog*. 2013;5(1):23. https://doi.org/10.1186/1757-4749-5-23.
39 Effendi RMRA, Anshory M, Kalim H, et al. *Akkermansia muciniphila* and *Faecalibacterium prausnitzii* in immune-related diseases. *Microorganisms*. 2022;10(12):2382. https://doi.org/10.3390/microorganisms10122382.
40 Chaudhari SN, Luo JN, Harris DA, et al. A microbial metabolite remodels the gut-liver axis following bariatric surgery. *Cell Host Microbe*. 2021;29(3):408-424.e7. https://doi.org/10.1016/j.chom.2020.12.004.
41 Funabashi M, Grove TL, Wang M, et al. A metabolic pathway for bile acid dehydroxylation by the gut microbiome. *Nature*. 2020;582(7813):566-570. https://doi.org/10.1038/s41586-020-2396-4.
42 Sonoda J, Xie W, Rosenfeld JM, et al. Regulation of a xenobiotic sulfonation cascade by nuclear pregnane X receptor (PXR). *Proc Natl Acad Sci U S A*. 2002;99(21):13801-13806. https://doi.org/10.1073/pnas.212494599.
43 You G, Yang R, Wei Y, et al. The detoxification effect of cytochrome P450 3A4 on gelsemine-induced toxicity. *Toxicol Lett*. 2021;353:34-42. https://doi.org/10.1016/j.toxlet.2021.10.003.
44 Sanada K, Nakajima S, Kurokawa S, et al. Gut microbiota and major depressive disorder: a systematic review and meta-analysis. *J Affect Disord*. 2020;266:1-13. https://doi.org/10.1016/j.jad.2020.01.102.
45 Vital M, Rud T, Rath S, et al. Diversity of bacteria exhibiting bile acid-inducible 7*α*-dehydroxylation genes in the human gut. *Comput Struct Biotechnol J*. 2019;17:1016-1019. https://doi.org/10.1016/j.csbj.2019.07.012.
46 Kim KH, Park D, Jia B, et al. Identification and characterization of major bile acid 7*α*-dehydroxylating bacteria in the human gut. *mSystems*. 2022;7(4): e0045522. https://doi.org/10.1128/msystems.00455-22.
47 Qu Q, Chen Y, Wang Y, et al. Lithocholic acid phenocopies anti-ageing effects of calorie restriction. *Nature*. 2025;643(8070):192-200. https://doi.org/10.1038/s41586-024-08329-5.
48 Pols TWH, Puchner T, Korkmaz HI, et al. Lithocholic acid controls adaptive immune responses by inhibition of Th1 activation through the vitamin D receptor. *PLoS One*. 2017;12(5):e0176715. https://doi.org/10.1371/journal.

pone.0176715.
49 Sheng W, Ji G, Zhang L. The effect of lithocholic acid on the gut-liver axis. *Front Pharmacol*. 2022;13:910493. https://doi.org/10.3389/fphar.2022.910493.
50 Choucair I, Nemet I, Li L, et al. Quantification of bile acids: a mass spectrometry platform for studying gut microbe connection to metabolic diseases. *J Lipid Res*. 2020;61(2):159-177. https://doi.org/10.1194/jlr.RA119000311.
51 Marksteiner J, Blasko I, Kemmler G, et al. Bile acid quantification of 20 plasma metabolites identifies lithocholic acid as a putative biomarker in Alzheimer's disease. *Metabolomics*. 2018;14(1):1. https://doi.org/10.1007/s11306-017-1297-5.
52 Staudinger JL, Goodwin B, Jones SA, et al. The nuclear receptor PXR is a lithocholic acid sensor that protects against liver toxicity. *Proc Natl Acad Sci U S A*. 2001;98(6):3369-3374. https://doi.org/10.1073/pnas.051551698.
53 Rizzo G, Renga B, Mencarelli A, et al. Role of FXR in regulating bile acid homeostasis and relevance for human diseases. *Curr Drug Targets Immune Endocr Metabol Disord*. 2005;5(3):289-303. https://doi.org/10.2174/1568008054863781.
54 Zelko I, Negishi M. Phenobarbital-elicited activation of nuclear receptor CAR in induction of cytochrome P450 genes. *Biochem Biophys Res Commun*. 2000;277(1):1-6. https://doi.org/10.1006/bbrc.2000.3557.
55 Lefebvre P, Chinetti G, Fruchart JC, et al. Sorting out the roles of PPARα in energy metabolism and vascular homeostasis. *J Clin Invest*. 2006;116(3):571-580. https://doi.org/10.1172/JCI27989.
56 Dong F, Perdew GH. The aryl hydrocarbon receptor as a mediator of host-microbiota interplay. *Gut Microbes*. 2020;12(1):1859812. https://doi.org/10.1080/19490976.2020.1859812.
57 Sun R, Chen M, Hu Y, et al. CYP3A4/5 mediates the metabolic detoxification of humantenmine, a highly toxic alkaloid from *Gelsemium elegans* Benth. *J Appl Toxicol*. 2019;39(9):1283-1292. https://doi.org/10.1002/jat.3813.
58 Denisov IG, Grinkova YV, McLean MA, et al. Midazolam as a probe for heterotropic drug-drug interactions mediated by CYP3A4. *Biomolecules*. 2022;12(6):853. https://doi.org/10.3390/biom12060853.
59 Tang AS, Brooks L, Boudreau DM, et al. Use of real-world claims data to assess the prevalence of concomitant medications to inform drug-drug interaction risk in target patient populations. *Clin Pharmacol Ther*. 2025;118(1):146-155. https://doi.org/10.1002/cpt.3652.
60 Zhai Q, Moes DJAR, van Gelder T, et al. The effect of genetic variants in the transcription factor TSPYL family on the CYP3A4 mediated cyclosporine metabolism in kidney transplant patients. *Clin Transl Sci*. 2024;17(2):e13729. https://doi.org/10.1111/cts.13729.
61 Liu Y, Zhang JW, Li W, et al. Ginsenoside metabolites, rather than naturally occurring ginsenosides, lead to inhibition of human cytochrome P450 enzymes. *Toxicol Sci*. 2006;91(2):356-364. https://doi.org/10.1093/toxsci/kfj164.
62 Kim SB, Cho SS, Cho HJ, et al. Modulation of hepatic cytochrome P450 enzymes by curcumin and its pharmacokinetic consequences in sprague-dawley rats. *Pharmacogn Mag*. 2015;11(Suppl 4):S580-S584. https://doi.org/10.4103/0973-1296.172965.
63 Yang C, Fang X, Zhan G, et al. Key role of gut microbiota in anhedonia-like phenotype in rodents with neuropathic pain. *Transl Psychiatry*. 2019;9(1):57. https://doi.org/10.1038/s41398-019-0379-8.
64 Li S, Huang J, Luo D, et al. Electro-acupuncture inhibits HDAC2 *via* modulating gut microbiota to ameliorate SNI-induced pain and depression-like behavior in rats. *J Affect Disord*. 2024;360:305-313. https://doi.org/10.1016/j.jad.2024.02.069.
65 Cheng R, Zhu H, Sun Y, et al. The modified outer membrane protein Amuc_1100 of *Akkermansia muciniphila* improves chronic stress-induced anxiety and depression-like behavior in mice. *Food Funct*. 2022;13(20):10748-10758. https://doi.org/10.1039/d2fo01198k.
66 Pinto-Sanchez MI, Hall GB, Ghajar K, et al. Probiotic *Bifidobacterium longum* NCC3001 reduces depression scores and alters brain activity: a pilot study in patients with irritable bowel syndrome. *Gastroenterology*. 2017;153(2):448-459.e8. https://doi.org/10.1053/j.gastro.2017.05.003.

This cover design illustrates the molecular mechanism by which comorbid depression severely exacerbates the neurotoxicity of *Gelsemium elegans* and its primary toxic constituent, humantenmine (HMT). In this visual narrative, the peripheral gut microbiota dysbiosis triggered by depressive stress is conceptualized at a microscopic level, revealing a pathological cascade wherein a precipitous decline in *Clostridium* abundance and its metabolite lithocholic acid downstream represses the activity of the primary hepatic metabolic enzyme CYP3A11. This obstruction of the gut–liver–brain metabolic axis ultimately leads to the catastrophic accumulation of HMT in brain tissues, thereby culminating in aggravated neurotoxicity. This visual representation serves as a profound scientific caveat: under complex conditions of multifaceted comorbidities, clinical administration of natural products or traditional Chinese medicines with narrow therapeutic windows demands heightened vigilance. Concurrently, this study provides a crucial theoretical foundation for the rational, safe utilization, and toxicity control of botanical medicines.